Influence of incidence angle on wear induced by sliding impacts

Emmanuel Rigaud, Alain Le Bot

Influence of Incidence Angle on Wear Induced by Sliding Impacts

Emmanuel RIGAUD, Alain LE BOT

Laboratoire de Tribologie et Dynamique des Systèmes, UMR CNRS 5513,

Ecole Centrale de Lyon, Université de Lyon

36, avenue Guy de Collongue

69134 ECULLY cedex

FRANCE

19 pages

11 figures

Abstract

Experiments are performed to analyze wear generated by low load sliding impacts on ferrite steel and stainless steel samples. Low load impacts are defined by a normal force such that the apparent contact pressure remains below the yield strength of the material. Nevertheless, concentration of pressure at the top of asperities may generate local plastic deformation. Beyond a running-in period, repetitive oblique impacts cause wear. A high frequency acquisition of dynamical contact forces allows an accurate characterization of impacts (rate, duration, strength) and forces (tangential and normal components and their ratio). These data are correlated with wear volume. The effect of the incidence angle is discussed. The results obtained confirm the combined effects of incidence angle and force ratio on the effective wear of impacts. An erosive wear model is introduced whose results explain all experimental observations. The normalized shear energy seems to be relevant in accounting for the measured evolution of wear with impacts orientation.

Keywords

Sliding impacts; Ductile materials; Time evolution of wear; Incidence angle; Erosion wear model; Normalized shear energy.

1- Introduction

Many devices used to guide mechanical parts or to transform motions and forces, are designed with functional clearances. External force fluctuation and excitation generated by contact between moving solids could lead to contact losses and dynamic response characterized by successive impacts. These ones can generate some wear leading to degradation of the mechanical systems durability. Wear induced by impacts is generally associated to erosion or percussion [1].

Erosion wear results from impacts of a large number of small particles with high impact velocity. It involves several wear mechanisms [2, 3]. Finnie [4, 5] published pioneering papers for understanding the erosion of ductile materials by impingement of hard particles and identified the main factors governing this form of wear. The influences of impact velocity, impact angle, particle shape and size have been clearly identified. Concerning impact angle, the wear rate depends on the target material. Ductile materials exhibit a maximum in the erosion rate for intermediate incidence angles (e.g. 60°-75°). In contrast, brittle materials exhibit a maximum in the erosion rate for normal impacts (i.e. incidence angle 0°) [6]. Corresponding predictive erosion wear models have been proposed in the literature [7, 8].

Percussion wear occurs for repetitive solid body impacts. For high load impacts, the initial impacts cause plastic deformation. The corresponding contact stresses exceed the fatigue limit. Subsurface cracks are formed and propagate due to delaminating of materials. The percussion wear was studied, for example, by Zanoria and Blau [9] who have enlightened the influence of incidence angle on wear of a brittle material (ceramic) subjected to repeated impacts using a simple ball-on-inclined-flat machine. Some corresponding predictive wear models have been developed from Hertz contact theory [10].

However, low load impacts generate an apparent contact pressure which remains below the yield strength of the materials. A wear process occurs near the surface, but this one is not yet well explained. Although the apparent contact pressure remains below the yield strength of the materials, the actual contact area is less than the apparent one and concentration of pressure at the top of asperities may generate local plastic deformation. So, impacts may result in the occurrence of wear, or not, depending on the contact angle. For example, for each unselected ratio of an automotive gearbox, the loose gear dynamic response is characterized by impacts with the opposite gears. The main drawback of this dynamic behaviour corresponds to the rattle noise emitted from the gearbox [11, 12]. But, successive impacts occur along the normal to contact surfaces. Despite a relative sliding between the surfaces, wear is not proven. For some other mechanical devices, the incidence angle of impacts is not null and unexpected wear occurs under far

less severe operating conditions than those from which it usually results: high applied load, high sliding velocity, corrosive environment, etc. Thus, premature wear has been observed for impacts between the cluster control rods and their guiding rings in nuclear power plants [13-17]. Similarly, wear has been observed in safety valves which equip the outlet pipe of the steam generators, due to impacts between the rod and its guiding rings [18]. This kind of impact wear has been much less studied and modelled than other wear processes.

In this study, experiments have been performed in order to generate and characterize low load dry sliding impacts. The evolution of the wear volume is analyzed and discussed in relation to the materials involved, the impact characteristics (e.g. their number and incidence angle), the normal and tangential contact forces. Then, an erosive wear model is introduced and corresponding results are compared to experimental ones.

2- Principle of experiment

The principle of the experiment is shown in Fig. 1. It is similar to the simple ball-on-inclined-flat machine previously used by Zanoria and Blau [9] who studied percussion wear of ceramics. A moving ball plays the role of impactor. It is fixed at the extremity of a thin cantilever beam which is submitted to flexural vibration imposed by a shaker. The input signal is supplied by a signal generator and a power amplifier. The excitation frequency (13 Hz) is chosen close to, but not at, the first natural frequency of the cantilever beam, in order to obtain large amplitude of the vertical displacement, while maintaining a low sensitivity of the response to change in external conditions. During its motion, the ball hits a plane steel sample placed in front of it. The ball is attached to the beam with a small compliant spring which induces a slight dispersion in impact location. The plane sample has a size of 15x15x5 mm. Its surface is prepared by polishing with diamond solution until the peak to peak roughness is less than 0.1 μm. The incidence angle θ between the normal to the sample surface and the vertical direction is adjustable to the values 30°, 50°, 60° and 70°, by changing the sample holder. Since the motion of the ball is mainly vertical, θ is also the mean value of impact angles.

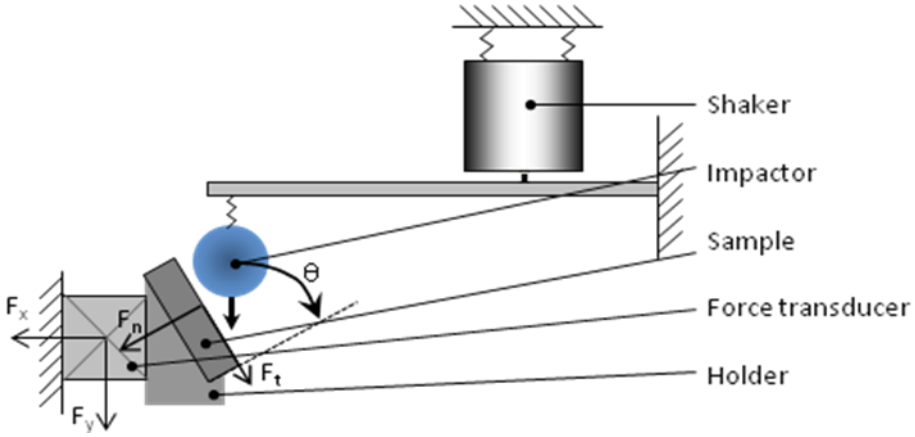

Fig. 1. Test rig.

3- Materials

Samples are made of two different materials. The first one is steel (C 0.1 %). The microstructure shows large ferrite grains (mass fraction 90%) with small islands of pearlite (mass fraction 10%). This steel has undergone a hardening leading to an increase in Vickers hardness to 200 Hv (under 3 kg). The nominal value of the yield point of the material is 670 MPa. The second material is an austenitic stainless steel type 304 (C 0.05 %, Cr 18 %, Ni 11 %) with Vickers hardness 145 Hv. The nominal value of the material yield point is 490 MPa. The impactor corresponds to a ball made of AISI 52100 steel with diameter 25.4 mm and Vickers hardness 800 Hv. Wear rate is assumed to be independent of the impactor hardness since it is at least twice that of the target material [19].

4- Measurement protocol

4.1 Impacts characteristics

The dynamic response of the impactor is characterized using a laser vibrometer. It is characterized by long free flights followed by short impacts during which the variation of velocity and contact force is very fast. The main impact is followed by multiple successive rebounds. The three components of the contact force are measured by a 3-axis piezoelectric force transducer placed behind the sample. The stiffness of the force transducer is 740 N/µm and the total mass of holder plus sample is 50 g. Thus, the contact force is accurately measured up to the frequency of 20 kHz. The signals are acquired by an analog/digital card with a sampling frequency of 50 kHz. This high value of sampling frequency ensures that the contact force is correctly measured during the impacts. Full records of force signals of duration 2 seconds are regularly done during the tests. As a result, the shock rate, duration of shocks, normal and tangential forces are obtained.

Fig. 2 displays the time evolution of the normal force during 1 second. The main impacts rate (6.5 impacts per second) differs from the excitation frequency, because the dynamical system is strongly nonlinear. The non-linearity comes from an initial gap, between the ball and the sample, which is about 1 mm at rest and from the nonlinear contact stiffness. It leads to a complex dynamic response of the ball [20, 21]. In these experiments, a periodic regime has been selected and the impact rate remains constant during the test. The total number of impacts is 560 000 for a 24 hours duration.

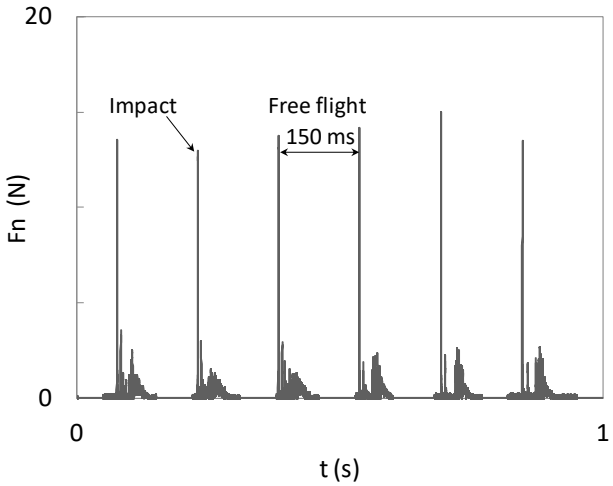

Fig. 2. Large scale time evolution of normal force F_n.

Fig. 3 displays the time evolution of the normal and tangential forces during one impact. Estimation of the impact duration from the normal or tangential force leads to similar results. Its mean value (0.4 ms) is very short compared to the period of the dynamic response (150 ms).

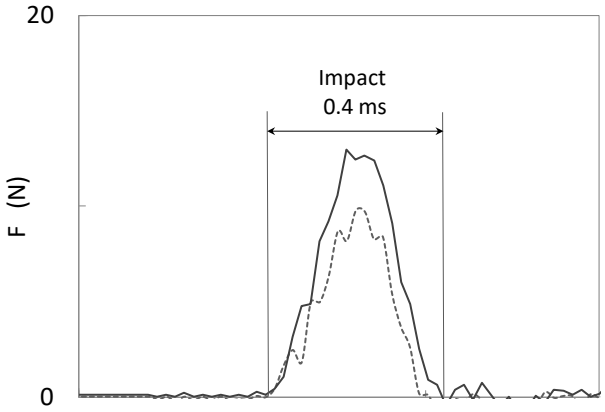

Fig. 3. Short scale time evolution of normal force F_n (——) and tangential force F_t (------) force during impact.

The excitation level is adjusted so that the mean value of the maximal normal force during impacts is equal to 13 N with a standard deviation equal to 3 N. An equivalent static contact modelled with the Hertz theory would have a contact diameter of 210 µm, a deflection of 0.8 µm larger than the initial roughness of surfaces and a maximum contact pressure of 290 MPa below the yield point of the material (670 MPa). However, the actual contact area is less than the apparent one and concentration of pressure at the top of asperities may generate local plastic deformation. From time evolution of the normal force during impacts, the impulse is defined as follows:

$$I = \int_{t_1}^{t_2} F_n(t)dt \quad (1)$$

where t_1 and t_2 are the respective start and stop times of the impact and F_n is the instantaneous normal force. The average value of impulse is 4 10^{-3} kg.ms^{-1}. From the mean impact velocity (50 mm s^{-1}), the impact duration (0.4 ms) and the incidence angle, the maximum sliding distance is estimated in between 10 and 20 µmn depending on the incidence angle.

In this paper, the instantaneous friction coefficient is defined as the ratio between simultaneous tangential and normal contact forces. It may be observed from Fig. 3 that this ratio is almost constant during the impact. So, in the remaining of this paper, the ratio between maxima of tangential and normal forces is retained to estimate the instantaneous friction coefficient. Notice that it may significantly differ from usual friction coefficient measured in steady sliding operating conditions. Furthermore, its value varies from one impact to another. However, this definition of friction coefficient is usually accepted in the field of erosive wear as long as there is sliding during impacts. In particular, it is meaningless for impacts with normal incidence.

4.2 Wear volume analysis

The total duration of the tests is 24 hours. The experiment can be interrupted several times, after 30 minutes, 1, 2, 4, 8 and 16 hours, in order to measure time evolution of wear volume. The sample is then removed. The test surfaces are first cleaned with heptane and then isopropyl alcohol in an ultrasonic bath for 10 minutes. Finally, the wear volume is carefully measured using surface topography devices and optical interferometer.

5- Results and discussion

5.1 Wear of ferrite steel sample and incidence angle 60°

As the contact between solids is of a very short duration, the studied impact wear is completely different from the other wear processes wherein the contact between the solids is continuous. Fig. 4 displays the wear trace topography observed at the plane sample surface and the corresponding profiles along two orthogonal lines after 24 hours. The ball surface is undamaged. The wear trace looks like a circular crater. Its diameter is *b*=1125 µm. This is larger than the impact contact area diameter and the sliding distance previously estimated, due to dispersion in impact locations.

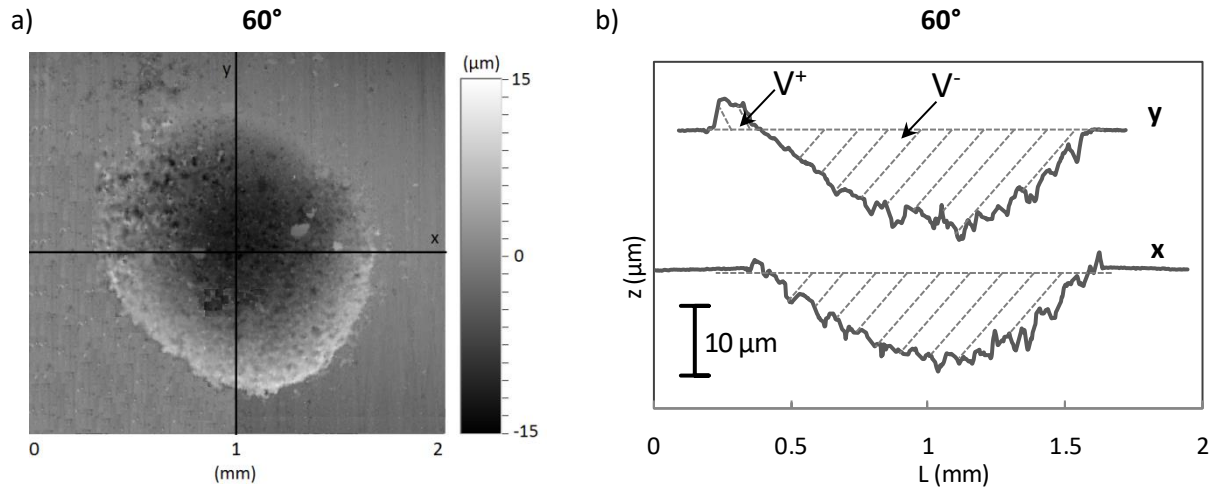

Fig. 4. Topography of the wear track and profiles along x and y, for test duration of 24 hours (ferrite steel).

The crater depth is *h*=12 µm. Its volume can be estimated assuming the crater corresponds to a part of a fictitious sphere. The radius *R* of the corresponding fictitious sphere is estimated from the crater diameter *b* and depth *h*:

$$R = \frac{b}{2\sin\alpha} \qquad \text{with} \qquad \alpha = 2\cos^{-1}\left(\frac{b}{\sqrt{b^2+4h^2}}\right) \qquad (2)$$

and the spherical cap volume is:

$$V^- = \pi h^2\left(R - \frac{h}{3}\right) \qquad (3)$$

This estimation leads to a final crater volume V^-=5.9 mm^3.This value is confirmed by direct measurement with optical 3D-interferometer (V^-=6.1 mm^3). A small portion of the ductile material has been displaced by plastic deformation outside the crater. A mound is formed and located below the crater due to the inclination of the sample and the ball kinematics. The positive volume corresponding to the mound is also measured with the optical interferometer (V^+=0.8 mm^3). The wear volume is defined as the difference

between the crater volume and the mound volume, that is to say V^{-}-V^{+}=5.3 mm^3. Almost 85% of the crater volume corresponds to wear. This value is confirmed by the weight loss of the sample (Δm=40 mg). The material is removed as wear debris rather than displaced.

5.2 Time evolution of wear, impact duration and friction coefficient (ferrite steel, incidence angle 60°)

Successive measurements of the profiles along two orthogonal lines after 30 minutes, 1, 2, 4, 8 16 and 24 hours are displayed in Fig 5. The corresponding time evolution of crater volume is displayed Fig. 6. The sample surface damaging process can be broken down as follows. Below 30 minutes (that is to say 12000 impacts), there is no significant evidence of plastic deformation at the surface, nor weight loss of the sample. After a critical number of impacts, that can be estimated at 24000 after 1 hour, a slight disturbance of the surface roughness appears due to repeated strain which causes metal fatigue, without generating crater or detectable wear. The initial roughness of the sample (0.1 µm peak to peak) rapidly rises until 3 µm peak to peak. This observation is consistent with the Engel model [22], which predicts a running-in period for a system subjected to sliding elastic impacts. Evolution of roughness leads to a modification in the real contact surface.

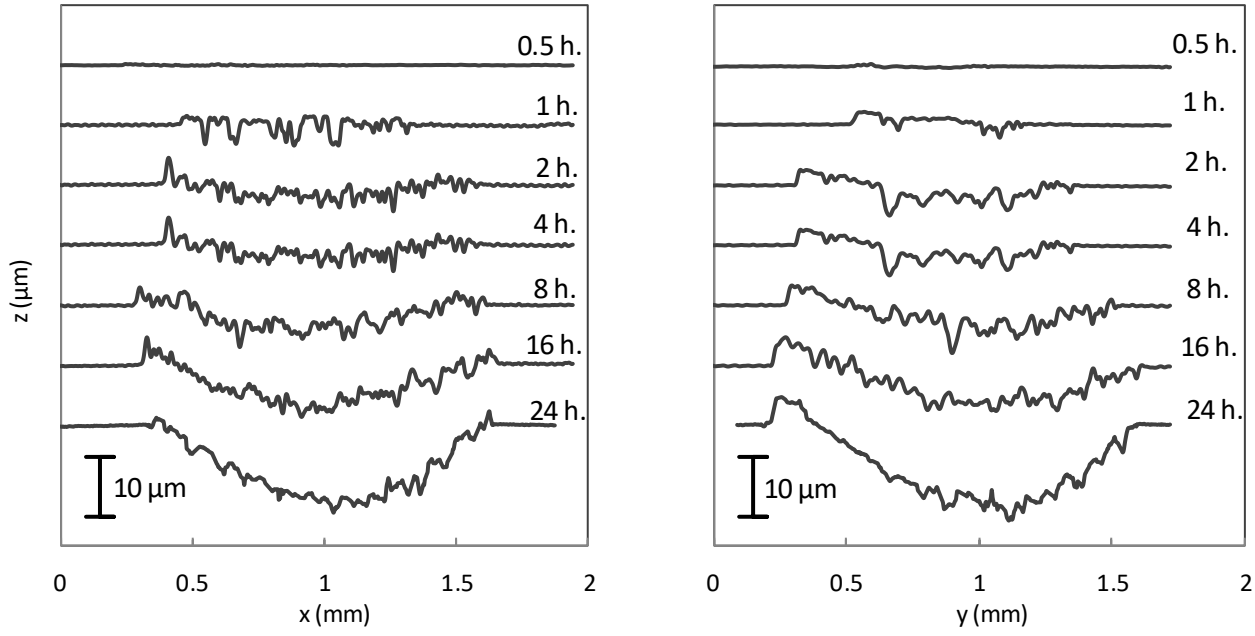

Fig. 5. Profiles measured along the horizontal and vertical diameters.

Test durations of 30 minutes, 1, 2, 4, 8, 16 and 24 hours.

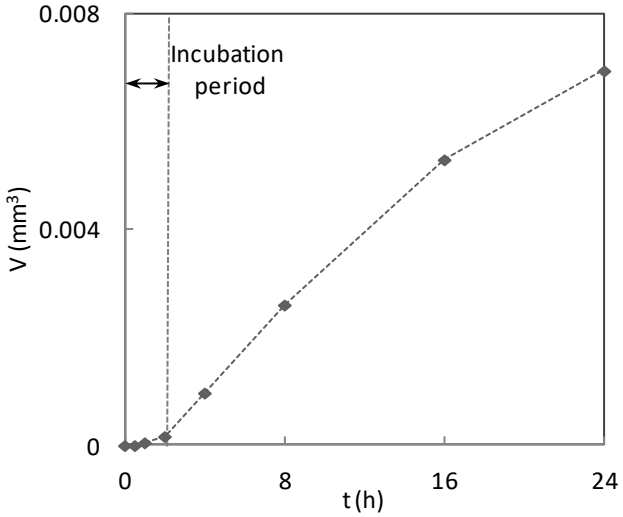

Fig. 6. Time evolution of the crater volume (incidence angle 60°, ferrite steel).

Beyond this running-in period, stress at impact may be sufficient to generate local plastic deformation at asperities and wear proceeds by surface fatigue. Visual observations show that wear debris escape from the contact zone under the influence of gravity. The crater volume increases almost linearly with the number of impacts. These experimental results are consistent with the wear model proposed by Levy et al. [23]. It predicts that wear is proportional to the number of impacts and a complex function involving friction coefficient, incidence angle and normal and tangential forces during impacts.

Evolution of impact duration and friction coefficient throughout the test has also been analyzed. The impact duration is almost constant at T=0.4 ms. The average value of friction coefficient increases from μ=0.5 to μ=0.7 during the running-in period. Then, once wear occurs, it remains almost constant at μ=0.7, with standard deviation 0.1, signifying that wear mechanisms remain the same during the rest of the test.

5.3 Effect of incidence angle

Similar experiments with ferrite steel samples have been performed using different holders, corresponding to mean impact incidence angles respectively equal to 30°, 50° and 70°. Experimental conditions did not permit exploration of incidence angles beyond 70°. Operating conditions have been chosen so that impulse defined from the time evolution of the normal force during impacts is almost the same for all experiments. The experiments are not interrupted before the total duration of 24 hours. Visual observations of wear debris flow shows that duration of the running-in period is almost independent of the incidence angle. The critical number of impacts is about 24000. Beyond the running-in period, a linear evolution of wear volume with the number of impacts is assumed, as observed for incidence angle 60°.

First, a significant increase in the average value of friction coefficient with incidence angle is observed (see Fig. 7). Standard deviation varies between 0.05 and 0.13. In the range of experimental incidence angles considered, a linear variation of average friction coefficient after the running-in period can be found:

$$\mu = 0.0117\ \theta \qquad (30° \leq \theta \leq 70°) \qquad (4)$$

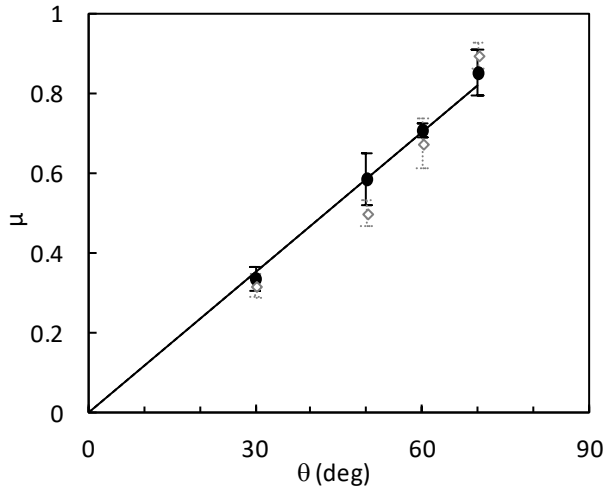

Fig. 7. Friction coefficient vs. incidence angle for ferrite steel (•) and stainless steel (o), the interval indicates the standard deviation amplitude for ferrite steel (I) and stainless steel (dashed I).

Preliminary experiment with normal impacts (incidence angle 0°) has shown there is no sliding and the tangential force is negligible during impacts. Neither crater nor roughness evolution are observed. Fig. 8 illustrates the change in topography after 24 hours for incidence angles varying from 30° to 70°. The following remarks can be made. For the 30° incidence angle, results show that the sample suffers a surface disturbance. A circular trace is observed for which the initial roughness has increased, but no crater is generated and no wear is detectable after 24 hours (see Fig. 8a). When the incidence angle is upgraded first to 50° and then to 60°, Fig. 8b and Fig. 4 show a significant increase in the crater diameter and depth. Then, a decrease is observed for the 70° incidence angle (see Fig. 8c).

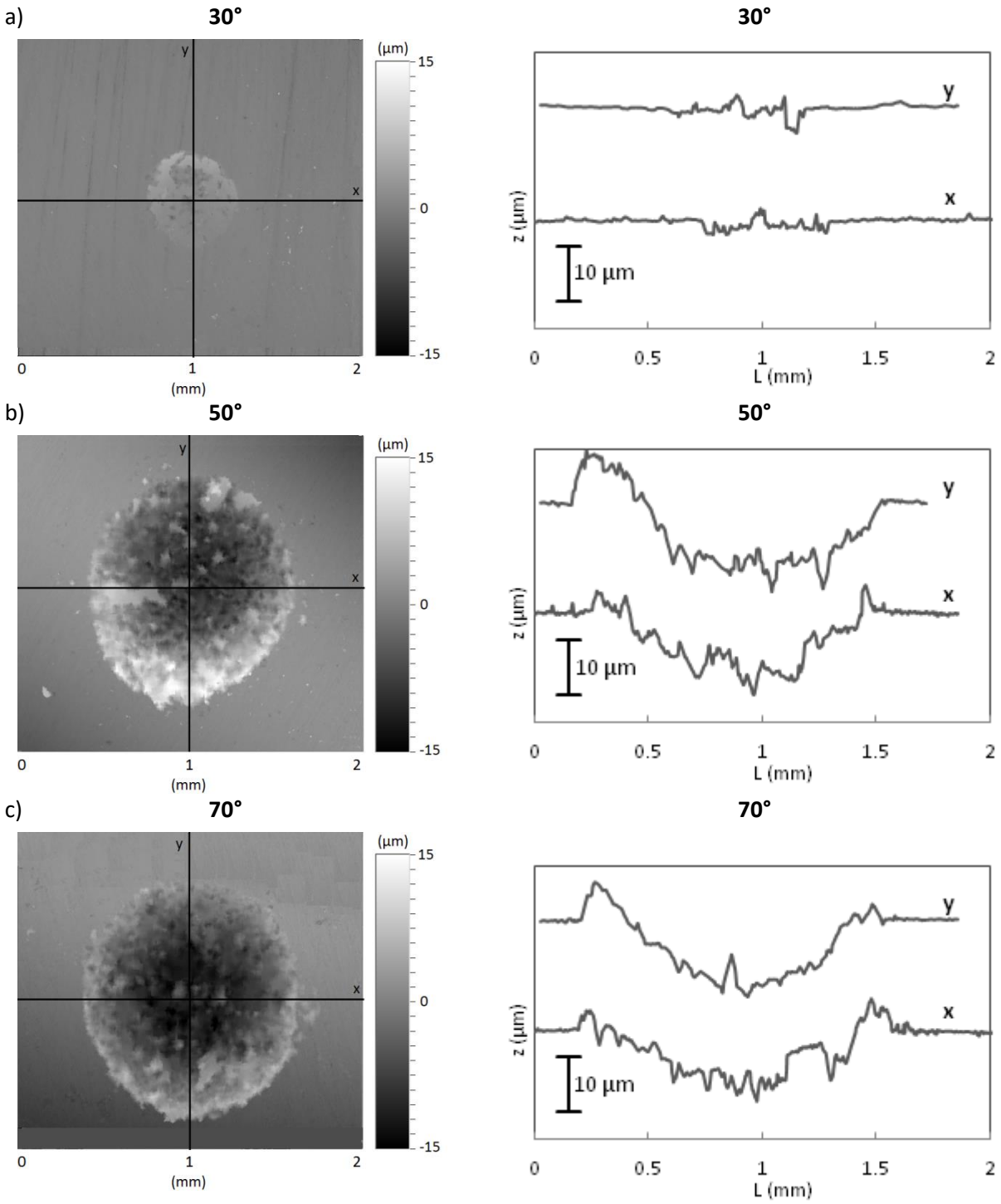

Fig. 8. Topography of the wear track and profiles along x and y, for test duration of 24 hours (ferrite steel).

Evolutions of the crater and wear volumes versus incidence angle have been measured with optical 3D-interferometer (Fig. 9). For all incidence angles, a small portion of the material is displaced into the form of a mound by plastic deformation. The main part of the material is removed as wear debris (between 75% and 85%). Both crater and wear volumes increase until 60° and then decrease for the 70° incidence angle.

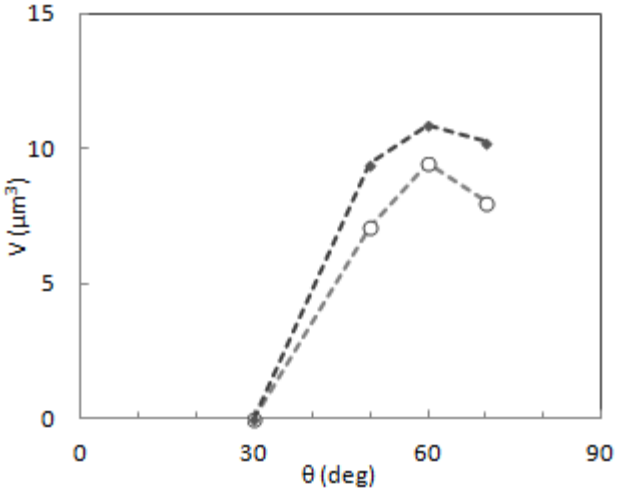

Fig. 9. Crater volume (♦) and wear volume (o) per impact vs. incidence angle (ferrite steel).

5.4 Influence of sample material

Similar experiments have been performed using 304 austenitic stainless steel samples in order to test the influence of the material. On the one hand, evolution of the friction coefficient versus incidence angle is similar to the one observed for the initial material (see Fig. 7). On the other hand, wear observed for stainless steel after 24 hours is significantly lower than wear observed for ferrite steel although the operating conditions remain the same. The wear rate depends on the material involved. Nevertheless, the analysis of intermediate results shows that the running-in period is identical to that observed for the ferrite steel and wear debris generation begins at the same time. As shown in Fig. 10, crater and wear volumes increase with incidence angle until 60° and then decrease for the 70° incidence angle. Results also confirm that the crater mainly results from material removal rather than plastic deformation.

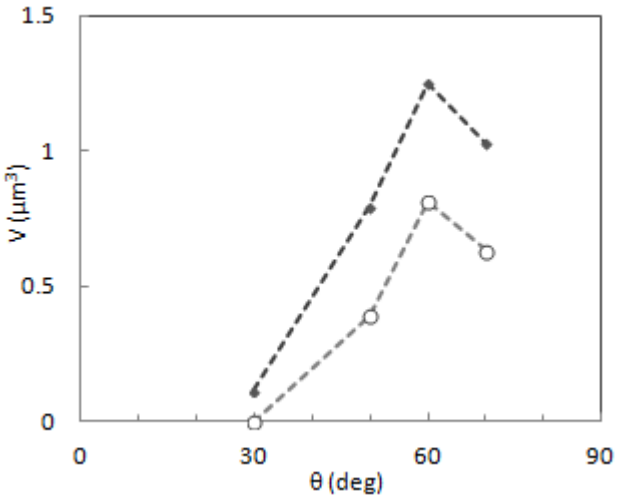

Fig. 10. Crater volume (♦) and wear volume (o) per impact vs. incidence angle (stainless steel).

5.5 Analysis based on impact wear models

From the analysis of low energy oblique impacts, Levy et al. [23] proposed a theoretical model for impact wear assuming the wear rate is related to the integral of the normal force by the sliding distance during impact. They estimated the dimensionless wear integral *J* as function of the approach angle ϕ, friction coefficient μ, and restitution coefficient of impacts *r*, taking into account the kinetic energy of the impacting solid:

$$J = \frac{\int F_n \, ds}{0.5 \, mV^2} = (1 + r) \, [\sin(2\phi) - (1 + r) \, \mu \sin^2(\phi)] \tag{5}$$

F_n is the instantaneous normal force, *m* and *V* are the impacting mass and velocity. The approach angle ϕ is related to the incidence angle θ as follows:

$$\phi = \left(\frac{\pi}{2} - \theta\right) \tag{6}$$

Introducing θ in Eq. (5) leads to:

$$J = (1 + r) \, \cos(\theta) \, [2 \sin(\theta) - (1 + r) \, \mu \cos(\theta)] \tag{7}$$

A second point of view is possible. From the study of erosion, Brach [7] and Sundararajan [8] have proposed a wear model also highlighting the combined effect of friction coefficient, restitution coefficient and approach angle of impacts. Erosion generally involves particles between 5 and 500 µm in size [3]. It seems to be far from low load sliding impacts between macroscopic solids because induced apparent contact area, pressure, size and velocity of involved solids are very different. Nevertheless, under low load such as that corresponding to the present experiments, contact is rather composed of several asperities whose size is comparable to those of erosive particles. Furthermore, kinetic energy of the macroscopic impactor with low velocity is similar to that of particles with high velocity, with an order of magnitude of 1 µJ in both cases. One can therefore expect that this erosive wear model is relevant to describe wear of macroscopic solids under low load impacts. Brach's model of erosive wear introduces a normalized shear energy *T** assumed to be the dimensionless energy transferred to target during an impact:

$$T^* = \frac{T}{0.5 \, mV^2} = \frac{1}{(1 + \lambda)} \, \frac{\mu}{\mu_c} \left(2 - \frac{\mu}{\mu_c}\right) \cos^2(\phi) \tag{8}$$

with

$$\mu_c = \frac{1}{(1 + \lambda)(1 + r)\tan(\phi)} \tag{9}$$

where μ_c is the critical friction coefficient and λ depends on the particle shape.

Applied to the problem considered in this study, λ and μ may be specified. Considering each asperity as a spherical particle that can be approximated by a point mass, we get λ=0. Furthermore, μ and θ are linked by the empirical law given eq. (4). Eq. (8) lead to:

$$T^* = (1+r)\,\mu(\theta)\,\cos(\theta)\,[2\sin(\theta) - (1+r)\,\mu(\theta)\cos(\theta)] \qquad (10)$$

The difference between normalized shear energy T^* and dimensionless wear integral J defined by Levy et al. takes into account the instantaneous friction force $\mu(\theta).F_n$ instead of the normal force F_n.

The restitution coefficient of impacts r is evaluated from Kadmiri et al. [12] who performed experiments to characterize restitution coefficient for impacts between sliding surfaces in the elastic domain. They highlighted that the restitution coefficient depends on antagonistic materials, impact velocity and presence or not of lubricant at the interface, but it is independent of sliding velocity between surfaces. A value consistent with experiments corresponding to a dry sphere-plane contact has been chosen (r=0.85).

Fig. 11 displays the evolution of the dimensionless wear integral J defined eq. (7) and the normalized shear energy T^* defined eq. (10) versus incidence angle θ. It can be seen that the normalized shear energy evolution agrees better with experiments than the wear integral. This result is coherent with experiments by Ko [13] which found the wear rate correlates well with the tangential force but neither with the normal force nor with the resultant force. There is often a threshold of the impacting particles velocity below which wear is negligibly small [3]. The lack of wear at 30° leads to the assumption of a normalized shear energy threshold equal to 0.25, below which the wear is insignificant. Fig. 11 highlights the increase in wear from an angle equal to 30° until a critical incidence angle close to 60°. Beyond this angle, the predicted wear decreases and becomes null for incidence angles close to 90°. This is in agreement with all experimental results for both materials. The ductile mode of erosive wear [3] prevails.

a)

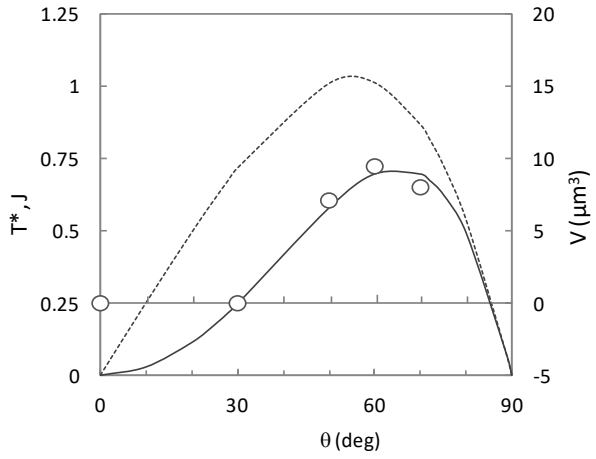

b)

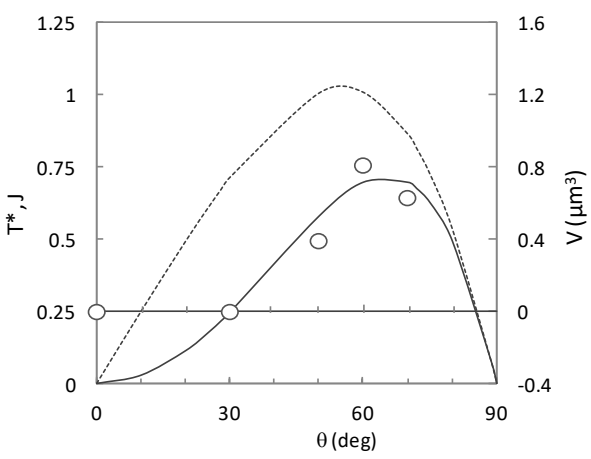

Fig. 11. Evolution of normalized shear energy T^* (———) and dimensionless wear integral J (-----) vs. incidence angle. Comparison of wear volume (o) for ferrite steel (a) and stainless steel (b).

6- Conclusion

Wear induced by impacts between a moving ball and steel samples whose incidence angle is adjustable has been analyzed. Experiments show that the interface submitted to sliding impacts is sensitive to wear, even for low energy impacts corresponding to an apparent contact pressure which remains below the yield point of the materials. Wear kinetics exhibits a running-in period resulting in a slight disturbance of the surface and a modification of roughness, but no detectable wear. The repetitive strain on the surface causes metal fatigue. During the running-in period, impact duration and friction coefficient both increase due to modification of the interface. Evolution of roughness leads to a decrease in the real contact area and an increase in the local pressure at the asperities. Beyond the running-in period, it is possible for the asperities to deform plastically on impact and wear occurs by repetitive plastic deformation. A crater begins to form mostly resulting from material removal, even if a slight portion is displaced by plastic deformation. Under the influence of gravity, a debris flow is observed outside the contact. The wear volume increases almost linearly with the number of impacts.

The experiments show that a change of the impact orientation leads to an increase in friction coefficient with incidence angle and also modifies the wear volume. An analogy with erosive wear is introduced. Beyond the running-in period, contact may occur at several asperities whose size is close to erosive particles. Furthermore, the kinetic energy involved in impacts is of the same order of magnitude as that of erosive particles. Thus, adopting an erosive model, the normalized shear energy defined by Brach is combined with the empirical law of friction coefficient versus incidence angle previously measured. The resulting evolution of normalized shear energy with impact orientation then explains all experimental observations. That is, no wear at low incidence angles, maximum of wear for incidence angle 60° and decrease in wear beyond an incidence angle of 70°. The normalized shear energy seems therefore to be relevant to describe wear of low load impacting solids.

7- References

[1] P. Engel, Impact wear of materials. Elsevier, New-York, 1978.

[2] E. Rabinowitz, The wear equation for erosion of metals by abrasive particles. 5th Conference on Erosion by Solid and Liquid impact, Cambridge, paper 38, 1-5, 1979.

[3] G.W. Stachowiak, A.W. Batchelor, Engineering Tribology, 3rd ed., Butterworth-Heinemann, Boston, 2005.

[4] I. Finnie, Some observations on the erosion of ductile metals. Wear 19(1), 81–90, 1972.

[5] I. Finnie, D.H. McFadden, On the velocity dependence of the erosion of ductile metals by solid particles at low angles of incidence. Wear 48(1), 181–190, 1978.

[6] G. Sundararajan, M. Roy, Solid particle erosion behaviour of metallic materials at room and elevated temperatures. Tribology International, 30(5), 339–359, 1997.

[7] R.M. Brach, Impact dynamics with applications to solid particles erosion. International Journal Impact Engineering, 7, 37-53, 1988.

[8] G. Sundararajan, A comprehensive model for the solid particle erosion of ductile materials. Wear, 149, 111-127, 1991.

[9] E.S. Zanoria, P.J. Blau, Effect of incidence angle on the impact-wear behavior of silicon nitride. Journal of American Ceramic Society, 81(4), 901–909, 1998.

[10] R. Blevins, Vibration induced wear of exchanger tubes. Journal of engineering materials and technology, 107, 61-67, 1983.

[11] K. Kariagiannis, F. Pfeiffer, Theoretical and experimental investigations of gear rattling. NonLinear Dynamics, 2 (5), 367-387, 1991.

[12] Y. Kadmiri, E. Rigaud, J. Perret-Liaudet, L. Vary, Experimental and numerical analysis of automotive gearbox rattle noise. Journal of Sound and Vibration, 331, 3144-3157, 2012.

[13] P.L. Ko, The significance of shear and normal force components on tube wear due to fretting and periodic impacting. Wear 106(1-3), 261-281, 1985.

[14] P.L. Ko, Wear of power plant components due to the impact and sliding. ASME Applied Mechanics Reviews, 50, 387-411, 1997.

[15] X. Delaune, E. De Langre, C. Phalipou, A probabilistic approach to the dynamics of wear tests. Journal of tribology, 122, 815-821, 2000.

[16] D. Kaczorowski, J.M. Georges, S. Bec, A. Tonck, A.B. Vannes, J.P. Vernot, Wear of a stainless steel in pressurised high temperature water. Comptes Rendus de l'Académie des Sciences, Series 4, Physics, 2(5), 739-747, 2001.

[17] A.L. Kaiser, S. Bec, J.P. Vernot, C. Langlade, Wear damage resulting from sliding impact kinematics in pressurized high temperature water. Journal of Physics D: Applied Physics, 39, 3193-3199, 2006.

[18] N. Brie, E. Luzzato, J.L. Lottiaux, E. Rigaud, A. Le Bot, Conception d'un batteur dynamique pour réduire l'usure des bagues de guidage de soupape GRISS. 18ème Symposium Vibrations, Chocs et Bruit, Lyon, 2010.

[19] A. Levy, Particle Erosion and Erosion-Corrosion of Materials. ASM International, 1995.

[20] E. Rigaud, J. Perret-Liaudet, Experiments and numerical results on non-linear vibrations of an impacting Hertzian contact. Part 1: harmonic excitation. Journal of Sound and Vibration, 265 (2), 289-307, 2003.

[21] J. Perret-Liaudet, E. Rigaud, Response of an impacting Hertzian contact to an order-2 subharmonic excitation: Theory and experiments. Journal of Sound and Vibration, 296 (1-2), 319-333, 2006.

[22] A. Engel, T. Lyons, J.L. Sirico, Impact wear model for steel specimen. Wear, 23 (2), 185-201, 1973.

[23] G. Levy, J. Morri, Impact wear in CO_2 base environment. Wear, 106 (1-3), 97-138, 1985.

List of figures